

# A Solid-State Dye-Sensitized Solar Cell Fabricated with Pressure-Treated P25–TiO<sub>2</sub> and CuSCN: Analysis of Pore Filling and IV Characteristics

Brian O'Regan,\* Frank Lenzmann, Ruud Muis, and Jeannette Wienke

*Solar Cells and Modules, Energy Research Center of the Netherlands,  
1755 ZG Petten, The Netherlands*

*Received May 16, 2002. Revised Manuscript Received September 12, 2002*

Solid-state dye-sensitized photovoltaic cells have been fabricated with TiO<sub>2</sub> as the electron conductor and CuSCN as the hole conductor. The cells show photocurrents of  $\approx 8$  mA/cm<sup>2</sup>, voltages of  $\sim 600$  mV, and energy efficiencies of  $\approx 2\%$  at 1 sun. The CuSCN was deposited into the pores of the nanoparticulate TiO<sub>2</sub>/dye film from dilute solution in propylsulfide. The degree of pore filling achieved is near 100% for TiO<sub>2</sub> films  $< 2\text{-}\mu\text{m}$  thick and falls to  $\approx 65\%$  for films near  $6\ \mu\text{m}$ . The final drying step after the CuSCN deposition is shown to be critical; drying in vacuum or argon is required for photocurrents above  $2\ \text{mA/cm}^2$ . The photocurrent IVs of these cells are fit to a single diode equation and the results are discussed and compared to those for equivalent photoelectrochemical cells, and similar solid cells composed of ZnO/dye/CuSCN.

## Introduction

Solid-state dye-sensitized solar cells are an offshoot technology of the dye-sensitized liquid-junction cells that have been under active development for the past decade.<sup>1–10</sup> Solid-state dye-sensitized cells have also been referred to as dye-sensitized heterojunctions (DSHs) by virtue of the placement of the light-absorbing dye at an otherwise transparent n–p heterojunction.<sup>11,12</sup> The promise of DSHs is the fusion of the inexpensive materials of the dye-sensitized liquid-junction technology with the easier and less expensive manufacturing and packaging applicable to solid devices. One of the proposed materials for the p-type side of a DSH is CuSCN.<sup>11,13,14</sup> The thiocyanate ion has also been investigated as a relay in dye-sensitized liquid-junction

cells.<sup>15</sup> In continuing our research into the combination TiO<sub>2</sub>/dye/CuSCN, we have constructed a large series ( $> 100$ ) of such cells utilizing only commercially available starting materials, with no further purification, and simple fabrication techniques. The fabrication techniques used are reasonably rapid and easily amenable to scale-up. The resulting cells show good currents and acceptable voltages, when compared to other solid-state dye-sensitized cells,<sup>16,17</sup> or to the related polymer/C-60 cells.<sup>18,19</sup>

The functioning of solid-state dye-sensitized devices has been described in the literature<sup>20</sup> and only a brief description will be included here (see Figure 1). The substrate was a commercial conductive SnO<sub>2</sub> glass. The SnO<sub>2</sub> was covered by spray pyrolysis with a thin ( $\sim 50$  nm) solid layer of TiO<sub>2</sub>, which prevents short circuiting between the SnO<sub>2</sub> and the CuSCN.<sup>21</sup> The active layer consists of a  $2\text{--}5\text{-}\mu\text{m}$  mesoporous TiO<sub>2</sub> layer, covered with a monolayer of a sensitizing dye, and then impregnated with CuSCN. The CuSCN also forms a layer above the TiO<sub>2</sub> film whose thickness we can vary

\* To whom correspondence should be addressed. E-mail: oregan@ecn.nl.

(1) Desilvestro, J.; Grätzel, M.; Kavan, L.; Moser, J.; Augustynski, J. *J. Am. Chem. Soc.* **1985**, *107*, 2988–2990.

(2) O'Regan, B.; Grätzel, M. *Nature* **1991**, *353*, 737–740.

(3) Nazeeruddin, M. K.; Péchy, P.; Renouard, T.; Zakeeruddin, S. M.; Humphry-Baker, R.; Comte, P.; Liska, P.; Cevey, L.; Costa, E.; Shklover, V.; Spiccia, L.; Deacon, G. B.; Bignozzi, C. A.; Grätzel, M. *J. Am. Chem. Soc.* **2001**, *123*, 1613–1624.

(4) Hirsch, A.; Kroon, J. M.; Kern, R.; Uhlendorf, I.; Holzbock, J.; Meyer, A.; Ferber, J. *Prog. Photovoltaics* **2001**, *9*, 425–438.

(5) van de Lagemaat, J.; Frank, A. J. *J. Phys. Chem. B* **2000**, *104*, 4292–4294.

(6) Haque, S. A.; Tacchibana, Y.; Willis, R. L.; Moser, J. E.; Grätzel, M.; Klug, D. R.; Durrant, J. R. *J. Phys. Chem.* **2000**, *104*, 538–547.

(7) Nogueira, A. F.; Durrant, J. R.; DePaoli, M. A. *Adv. Mater.* **2001**, *13*, 826–830.

(8) Kuciauskas, D.; Freund, M. S.; Gray, H. B.; Winkler, J. R.; Lewis, N. S. *J. Phys. Chem. B* **2001**, *105*, 392–403.

(9) Gillaizeau-Gauthier, I.; Odobel, F.; Alebbi, M.; Argazzi, R.; Costa, E.; Bignozzi, C. A.; Qu, P.; Meyer, G. J. *Inorg. Chem.* **2001**, *40*, 6073–6079.

(10) Gregg, B. A.; Pichot, F.; Ferrere, S.; Fields, C. L. *J. Phys. Chem. B* **2001**, *105*, 1422–1429.

(11) O'Regan, B.; Schwartz, D. T. *Chem. Mater.* **1995**, *7*, 1349–1355.

(12) O'Regan, B.; Schwartz, D. T. In *Nanostructured Materials in Electrochemistry*; Searson, P. C., Meyer, G. J., Eds.; The Electrochemical Society: Pennington, NJ, 1995; pp 208–211.

(13) Kumara, G. R. R. A.; Konno, A.; Senadeera, G. K. R.; Jayawera, P. V. V.; De Silva, D. B. R. A.; Tennakone, K. *Sol. Energy Mater. Sol. Cells* **2001**, *69*, 195–199.

(14) Tennakone, K.; Kahanda, M.; Kasige, C.; Abeysooriya, P.; Wijayanayaka, R. H.; Kaviratna, P. *J. Electrochem. Soc.* **1984**, *131*, 1574–1577.

(15) Oskam, G.; Bergeron, B. V.; Meyer, G. J.; Searson, P. C. *J. Phys. Chem.* **2001**, *105*, 6867–6873.

(16) Krüger, J.; Plass, R.; Cevey, L.; Piccirelli, M.; Grätzel, M.; Bach, U. *Appl. Phys. Lett.* **2001**, *79*, 2085–2087.

(17) Kumara, G. R. A.; Konno, A.; Shiratsuchi, K.; Tsukahara, J.; Tennakone, K. *Chem. Mater.* **2002**, *14*, 954–955.

(18) Shaheen, S. E.; Brabec, C. J.; Sariciftci, N. S.; Padinger, F.; Fromherz, T.; Hummelen, J. C. *Appl. Phys. Lett.* **2001**, *78*, 841–843.

(19) Kroon, J. M.; Wienk, M. M.; Verhees, W. J. H.; Hummelen, J. C. *Thin Solid Films* **2002**, *403*, 223–228.

(20) O'Regan, B.; Schwartz, D. T. *Chem. Mater.* **1998**, *10*, 1501–1509.

(21) O'Regan, B.; Schwartz, D. T. *J. Appl. Phys.* **1996**, *80*, 4749–4754.

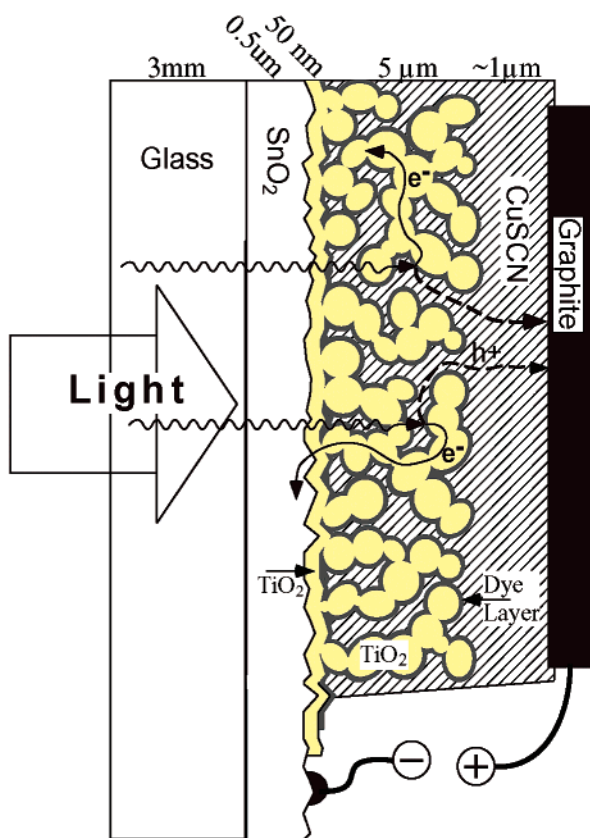


**Figure 1.** Schematic of a solid-state dye-sensitized photovoltaic cell.

between 0.2 and 3  $\mu\text{m}$ . The electrical contact to the CuSCN is made with pressed graphite or evaporated gold, both of which give similar results.

After a photon is absorbed by the dye, the excited state is quenched by electron injection into the  $\text{TiO}_2$  conduction band. The thus photo-oxidized dye is then regenerated by capture of an electron from the valence band of CuSCN, a process also referred to as hole injection. (It is also possible that the hole injection occurs first, followed by the reduced dye injecting an electron into  $\text{TiO}_2$ .) The two photoseparated charges then percolate through the two phases and, in the absence of recombination, reach the  $\text{SnO}_2$  and back contact, respectively. Recombination consists of either (a) reduction of the oxidized dye by an electron from  $\text{TiO}_2$  before hole injection into CuSCN regenerates the dye or (b) recombination of an electron from the  $\text{TiO}_2$  with a hole in the CuSCN. It should be kept in mind that Figure 1 is a schematic. The 5- $\mu\text{m}$ -thick  $\text{TiO}_2$  films used herein are  $\approx 200$  particles thick. By analogy to liquid-junction dye-sensitized cells, the electron path through the film is probably a random walk. If so, the number of  $\text{TiO}_2$  particles visited by a single electron is on the order of 10 000, not at all as we have drawn in Figure 1.

### Methods

Transparent conductive  $\text{SnO}_2$  glass, "LOF Tec 8", nominal resistance 8  $\Omega/\text{sq.}$ , was purchased from Pilkington. A thin solid film of  $\text{TiO}_2$  (30–100 nm) was deposited on the  $\text{SnO}_2$  by spray pyrolysis.<sup>21</sup> Mesoporous  $\text{TiO}_2$  layers were pressed onto the spray layer using an approach based on that of Lindström et

al.<sup>22</sup> First, 2 g of  $\text{TiO}_2$  powder (Degussa P25, average diameter 25 nm) was suspended in 10 mL of pure ethanol by stirring for several hours followed by 5 min of sonication using a titanium horn immersed in the suspension. The sonication duty cycle was 25% or less to avoid overheating and evaporation of the ethanol. The slurry was spread onto the surface of the  $\text{SnO}_2/\text{TiO}_2$  substrate by tape casting (doctor blading) using one or more layers of scotch tape (50  $\mu\text{m}$ ) as spacers. The resulting layer of ethanol/ $\text{TiO}_2$  was allowed to dry in the ambient atmosphere. The very loose film of particles that results was then pressed between two steel plates at 500  $\text{kg}/\text{cm}^2$  for 60 s. Under such pressures, similar P25 films have been found to compress significantly, decreasing from an initial porosity of over 80% to about 60%.<sup>22</sup> To avoid adhesion of the  $\text{TiO}_2$  to the steel plate, several materials were used to cover the  $\text{TiO}_2$  film during pressing; carbon paper, aluminum foil, and polyethylene all work to some extent. Despite this, in many cases some of the compressed  $\text{TiO}_2$  film adheres to the cover instead of the substrate. If the film does not pull off with the cover material, the adhesion to the substrate is subsequently excellent. In general, the films cannot be removed by a stream of water or air, but can be removed by rubbing lightly.

$\text{TiO}_2$  layer thickness after pressing was varied from 1 to 7.5  $\mu\text{m}$  depending on the slurry concentration and number of spacer tape layers. The  $\text{TiO}_2$  layers were then heated for 2 h at 500  $^\circ\text{C}$  in air. Films were removed from the oven at  $\approx 100$   $^\circ\text{C}$  and placed in ethanolic solutions of the dye "N3", which is  $\text{RuL}_2(\text{SCN})_2$  where L = 4,4'-dicarboxy-2,2'-bipyridine. The dye was purchased from Solaronix under the name Ruthenium 535. In this form, the dye is intended to have four protons as counterions. After being dyed overnight, the films were rinsed in ethanol and dried in a stream of compressed air. Electrodes were then weighed, to allow the later determination of the quantity of CuSCN deposited. The weighing involved a certain amount of time of exposure to wet air. This time was normally in the range of 20–120 min.

To make the CuSCN deposition solution, 0.2 g CuSCN was placed in 10 mL of propylsulfide,  $(\text{CH}_3\text{CH}_2\text{CH}_2)_2\text{S}$ . Both chemicals were purchased from Aldrich and used as received. The solution was stirred overnight and then allowed to settle for at least 1 additional day. The amount added is just slightly over the solubility at room temperature. Aliquots of 2 mL were removed from the supernatant and diluted with an additional 150  $\mu\text{L}$  of propylsulfide before being used for deposition of CuSCN films.

Deposition of the CuSCN into the pores of the  $\text{TiO}_2$  was carried out using a modification of the method proposed by Kumara et al.<sup>13</sup> The dried and weighed  $\text{TiO}_2$ /dye electrode was placed on a copper plate heated to 80  $^\circ\text{C}$  by an underlying hot plate. The temperature of the plate was held to within 2  $^\circ\text{C}$  of 80  $^\circ\text{C}$ . The plate and sample were placed at the entrance of a common chemical hood with the cover open as far as possible. This resulted in a slow flow of air across the surface. Very thin films of the CuSCN solution ( $\approx 1.2$   $\mu\text{L}/\text{cm}^2$ ) were then spread onto the surface and allowed to dry. The boiling point of propylsulfide is 142  $^\circ\text{C}$ . Each film required about 12 s; thus, 50 films could be applied in  $\approx 10$  min. The CuSCN solution was placed onto the surface somewhat above room temperature due to the proximity of the applying needle to the hot plate, but the actual temperature was impossible to measure due to the very small volume involved. Due to the air flow and evaporation of the solvent, the surface of the electrode during CuSCN deposition was certainly below 80  $^\circ\text{C}$ , though this has also not been measured.

For a 5- $\mu\text{m}$   $\text{TiO}_2$  film, 60–70 applications were required to deposit a sufficient quantity of CuSCN so that the pores were "filled" and an approximately 1- $\mu\text{m}$  layer of CuSCN built up on top of the  $\text{TiO}_2$  film. As shown in the Results section, much of the CuSCN ends up inside the pores of the  $\text{TiO}_2$ . The resulting composite cells were either allowed to dry in air, or

(22) Lindström, H.; Magnusson, E.; Holmberg, A.; Södergren, S.; Lindquist, S. E.; Hagfeldt, A. *Solar Energy Mater. Solar Cells* **2002**, *73*, 91–101.

argon, for several days or were treated under “low” vacuum ( $\approx 5 \times 10^{-2}$  Torr) for 2 h. The cells were weighed before and after the CuSCN application to find the weight of the added CuSCN. The thicknesses of the porous  $\text{TiO}_2$  film and the subsequent  $\text{TiO}_2/\text{CuSCN}$  composite were measured by profilometry. The thickness of the CuSCN overlayer above the  $\text{TiO}_2$  film was found by subtraction. Assuming that the CuSCN overlayer is nonporous (density  $2.85 \text{ g/cm}^3$ ), the weight of the CuSCN above the  $\text{TiO}_2$  could be found. Subtracting this value from the total weight of CuSCN gave the weight and volume of CuSCN in the pores of the  $\text{TiO}_2$  film. With use of the porosity of the  $\text{TiO}_2$  films, the fraction of the porosity that was filled with CuSCN could be calculated.

Photocurrent vs voltage measurements were taken using illumination from a Steuernagel solar simulator. The Steuernagel contains a 575-W “metal halide” bulb. This bulb is essentially a mercury lamp with added rare earth halides. A peak at 370 nm gives this bulb relatively more UV light than the AM1.5 spectrum. Due to this, the photocurrent measurements will contain some error due to spectra mismatch, and thus the measured efficiencies are not presented as fully calibrated values.

The dark and photo IVs have been fit to a single exponential (a “diode model”) incorporating a shunt and a series resistance:

$$J = J_p - Ke^{\alpha V_i} - (C_{sh} V_i) \quad (1)$$

$$V_{ext} = V_i + (JR_{ser}) \quad (2)$$

where  $J_p$  is the photocurrent,  $V_i$  is the cell internal voltage,  $V_{ext}$  is the measurement voltage, and  $C_{sh}$  is the shunt conductivity. Although the structure of the device is much more complicated than a single diode, the IV data can be fit very closely with this equation. Typically, the average absolute residual is  $<1\%$  of the current range. We do not argue that the diode equation model parameters have direct physical meaning for our system. For example, it is reasonably certain that the CuSCN and  $\text{TiO}_2$  will have different conductivities under operation, so the full cell should be modeled as a stack of subcells, each with a different  $R_{ser}$ . Similar arguments apply to the other parameters. For this reason, whereas diodes are frequently discussed in terms of their “ideality factor”, equal to  $1/(\alpha kT)$ , we will report only  $\alpha$  herein to avoid direct comparison with normal diodes. Despite these concerns, the fit parameters are useful for general discussion of the shape of the IV curves and possible improvements therein.

## Results and Discussion

**IV Results.** Figure 2 shows some typical IVs produced by  $\text{TiO}_2/\text{dye}/\text{CuSCN}$  DSHs. In Figure 2 the solid lines are the measured data, and the dotted lines are the fits using the diode equation as described in the Methods section. (In some parts of the graph the fits are not visible as they lie directly on the data.) The IV results and model parameters for this and several other cells are summarized in Table 1. The dark current curves typically show good diode characteristics with low shunt conductivities ( $C_{shunt}$  in Table 1). For the example shown in Figure 2 the dark  $C_{shunt}$  is  $0.08 \text{ mS}$  for a  $1\text{-cm}^2$  surface. Under 1 sun illumination, the cell in Figure 2 produced a short circuit current of  $7.8 \text{ mA/cm}^2$ . Along with the voltage of  $0.59 \text{ V}$ , and fill factor of  $0.44$ , this results in an energy efficiency of  $2\%$  at 1 sun. The photocurrent was linear with light intensity over the range  $60\text{--}1000 \text{ W/m}^2$ .

We have measured several cells which produced short circuit current densities of  $\approx 8 \text{ mA/cm}^2$ , at  $1000 \text{ W/m}^2$  illumination, and gave IVs resembling those in Figure 2. However, we have found some variation in the IV

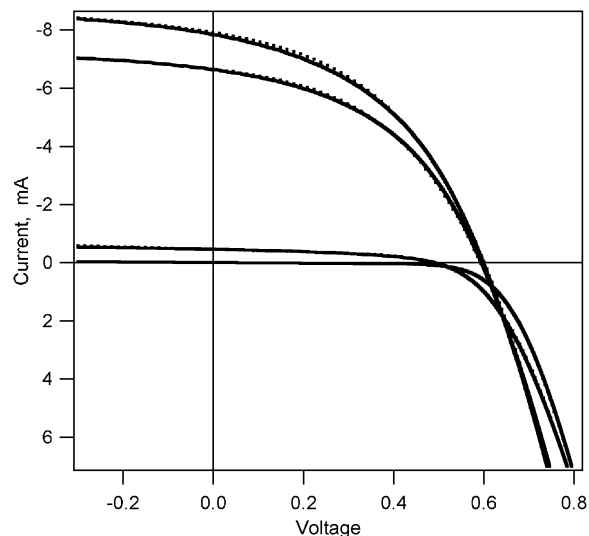


**Figure 2.** IV characteristics of a “type A”  $\text{TiO}_2/\text{N3}/\text{CuSCN}$  cell. Solid lines from top to bottom: cell output under  $1000 \text{ W/m}^2$ ,  $850 \text{ W/m}^2$ ,  $60 \text{ W/m}^2$ , and dark. Light source described in the Methods section. Dotted lines: fits of the data with a diode equation, as described in the text.  $\text{TiO}_2$  thickness  $5.8 \mu\text{m}$ ; area  $1 \text{ cm}^2$ .

curves between cells with identical  $\text{TiO}_2/\text{dye}$  layers and no intentional differences in the CuSCN deposition. These differences include  $\approx 20\%$  variation in the photocurrent and fill factor, as well as changes in the linearity and series resistance. The variations in the different IV characteristics do not seem to be independent of each other, but rather vary together to form a series of possible cell types. To illustrate and discuss these differences, we have chosen a “matched pair” of cells, made on the same day with the same procedures, which lie near the extremes of this variation. We will refer to the type of cell in Figure 2 as “type A”, to be compared to “type B” in Figure 3.

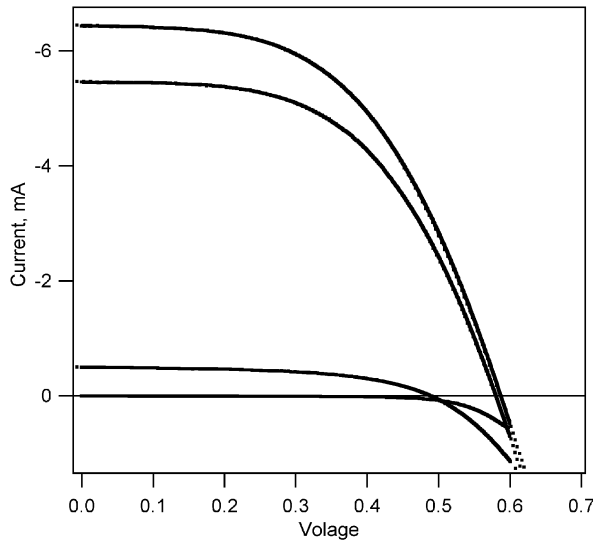
In Figure 2, it is clear that the low fill factor is an important limitation on the efficiency. The fill factor is degraded by the “flattened” shape of the IV at 1 sun, relative to the higher curvature in the dark current. This flattening of the curvature shows up in the fit parameters as a decrease in the value of  $\alpha$  in equation 1. For the example shown in Figure 2,  $\alpha$  decreases from 22 for the dark current to 5.8 for the 1 sun measurement. (This corresponds to an increase in the “ideality factor” from 1.8 to 6.8.) If, under 1 sun, the cell maintained the  $\alpha$  value of the dark current, as is observed in optimized dye-sensitized liquid-junction cells, the fill factor would be  $0.65$  and the efficiency  $2.4\%$ .

The IVs in Figure 2 also show evidence for a photoshunt, which increases with illumination intensity (see Table 1). However, at 1 sun the photoshunt is not a major loss factor. Eliminating the photoshunt from the 1 sun fit curve results in a change of the fill factor only from  $0.44$  to  $0.45$ . At lower light levels, however, the photoshunt can become important. For the cell shown in Figure 2, at  $60 \text{ W/m}^2$  ( $6\%$  sun), it is the photoshunt which limits the fill factor. Eliminating the photoshunt from the model curve results in an improvement of the fill factor to  $0.58$ . At this light level,  $\alpha$  is 15, and the contribution of  $\alpha$  to the low fill factor is less important.

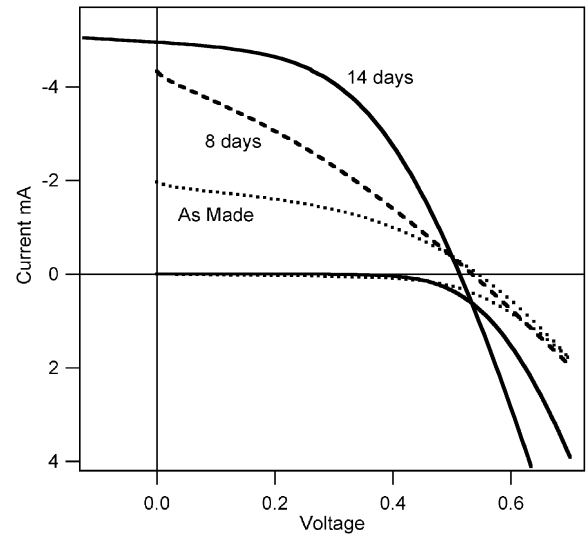
Figure 3 shows a typical set of IVs for a cell of “type B”. The most striking difference between the two sets

**Table 1. Photocurrent, and Dark Current, vs Voltage Values for 1-cm<sup>2</sup> Solid and Liquid-Junction Dye-Sensitized Cells, and Fit Parameters for the One-Diode Model**

cell	measured					modeled			
	illumin.(W/m <sup>2</sup> )	$J_{sc}$ (mA/cm <sup>2</sup> )	$V_{oc}$ (V)	fill factor	eff. (%)	$\alpha$	$-\log(K)$	$C_{shunt}$ (mS)	$R_{ser}$ ( $\Omega$ )
type A	dark					22	8.7	0.08	12
	60	0.46	0.49	0.42	1.5	15	6.7	0.4	11
	850	6.6	0.59	0.45	2.1	7	3.9	0.85	6
	1000	7.8	0.60	0.44	2.1	5.8	3.7	1.0	5
type B	dark					25	9.6	0.01	16
	60	0.5	0.49	0.54	2.2	14	6.3	0.1	16
	850	5.5	0.58	0.54	2.1	13	5.6	0.3	15
	1000	6.4	0.59	0.52	2.0	12	4.9	0.3	13
liquid junction	dark					18	6.4	<0.1	11
	120	1.5	0.39	0.57	2.8	13	5.0	<0.1	11
	1000	11.8	0.49	0.41	2.35	9	4.0	<0.1	11
ZnO	dark					24	7.9	0.12	33
	30	0.1	0.39	0.57	0.74	24	8.2	0.05	37
	1000	3.1	0.53	0.55	0.9	24	8.1	0.3	36

**Figure 3.** IV characteristics of a “type B” TiO<sub>2</sub>/N3/CuSCN cell. Solid lines from top to bottom: cell output under illumination with 1000 W/m<sup>2</sup>, 850 W/m<sup>2</sup>, 60 W/m<sup>2</sup>, and dark. Light source described in the Methods section. Dotted lines: fits of the data with a diode equation, as described in the text. TiO<sub>2</sub> thickness 5.8  $\mu$ m; area 1 cm<sup>2</sup>.

of IVs is the improvement in the fill factor to 0.52, and the related plateau in the IVs at all light levels, which are found for the type B cell shown in Figure 3. The photocurrents are also somewhat lower for the type B cell, but the higher fill factor, and the lower photoshunt, result in the same energy efficiency as for type A cells. As the SnO<sub>2</sub> substrate and TiO<sub>2</sub> film were identical for the two cells, the changes between the A and B type cells must be related to differences in the CuSCN layer. It is also notable that the lower 1 sun photocurrent in the type B cell is due to the fact that the photocurrent is sublinear with respect to light level (77% between 60 and 850 W/m<sup>2</sup>). At 60 W/m<sup>2</sup> the photocurrent from the type B cell is in fact higher than that for type A. Had the cell shown in Figure 3 been linear, as is that in Figure 2, the 1 sun photocurrent would have been 8.3 mA. The plateau in both the low and high light IVs, in Figure 3, shows that the nonlinearity is not caused by the series resistance. Possible causes for this nonlinearity will be discussed in the section on drying, below. In addition, for the cell in Figure 3, the series resistance is more than twice as high as that in Figure 2. Without

**Figure 4.** Dark and photo IV characteristics of a TiO<sub>2</sub>/N3/CuSCN cell under argon storage (with no prior vacuum treatment). Illumination intensity 850 W/m<sup>2</sup>. TiO<sub>2</sub> thickness 3.5  $\mu$ m; area 1 cm<sup>2</sup>.

this higher series resistance, the higher  $\alpha$  value for the type B cell would give rise to a fill factor of 0.59.

The data shown in Figures 2 and 3 were taken after the vacuum treatment and several days storage in an argon atmosphere. Cells tested before vacuum treatment typically show very high series resistance ( $>100 \Omega$ ), and short circuit photocurrents that are clearly limited by this resistance. Before vacuum treatment, maximum short circuit photocurrents are  $\approx 2$  mA/cm<sup>2</sup>. In some cases cells have shown high photocurrents immediately after vacuum treatment, but in most cases several more days of drying in argon was required to reach maximum current. All cells show an improvement in fill factor with storage in argon. The 1-h vacuum treatment can be replaced by much longer storage in dry argon. Figure 4 shows the IVs immediately after fabrication, and the effect of argon storage for 8 and 14 days. Initially, and after 8 days, the photocurrent is clearly limited by the series resistance. After 14 days the series resistance has decreased and the photocurrent shows a plateau. After 2 weeks, continued storage in argon does not cause further large changes.

We have also compared TiO<sub>2</sub>/N3/CuSCN cells with standard dye-sensitized liquid-junction cells using the

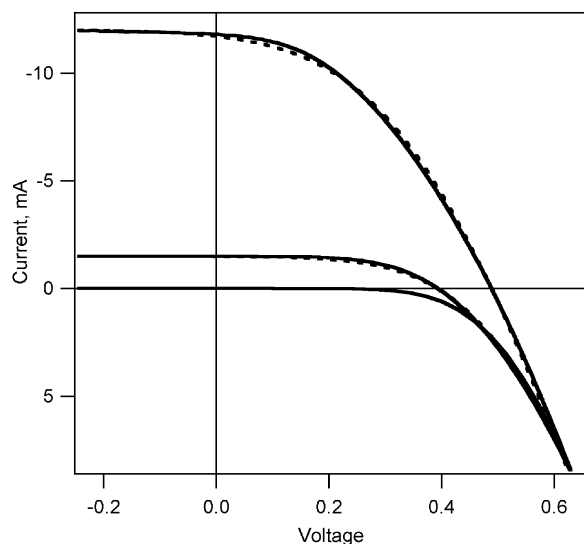


**Figure 5.** Dark and photo IVs for a liquid-junction cell fabricated using an identical  $5.8\text{-}\mu\text{m}$   $\text{TiO}_2/\text{N3}$  film as used in Figures 2 and 3. Electrolyte was methoxypropionitrile with  $0.4\text{ M}$  lithium iodide and  $20\text{ mM}$  iodine. Illumination, top to bottom:  $1000\text{ W/m}^2$ ,  $120\text{ W/m}^2$ , and dark.. Dotted lines: diode equation fits, as described in the text.  $\text{TiO}_2$  thickness  $5.8\text{ }\mu\text{m}$ ; area  $1\text{ cm}^2$ .

same  $\text{TiO}_2$  and N3 layers. The measurements were conducted in a sandwich-type cell, with an electrolyte of methoxypropionitrile,  $0.4\text{ M}$  lithium iodide, and  $20\text{ mM}$  iodine. The lithium-containing electrolyte was chosen to maximize the photocurrent output of the cell, at the expense of voltage. Experience has shown that, with this electrolyte, the quantum efficiency for current generation from absorbed photons (internal quantum efficiency) is  $\geq 90\%$ . The results are presented in Figure 5. Two things are apparent from the comparison of the electrochemical cell and the DSH. (See also Table 1.) First, comparison of the photocurrent of the DSH ( $7.8\text{ mA}$ ) with that of the electrochemical cell ( $11.8\text{ mA}$ ) implies that the internal quantum efficiency for the DSH is  $\approx 66\%$ . Second, it is apparent that the fill factor of the liquid-junction cell,  $48\%$ , is not as high as the  $65\text{--}70\%$  found for liquid-junction cells fabricated from colloidal  $\text{TiO}_2$ . Lindström et al. have also reported low fill factors for dye-sensitized liquid-junction cells from pressed P25 films.<sup>22</sup> From this we conclude that some part of the low fill factor shown by the  $\text{TiO}_2/\text{N3}/\text{CuSCN}$  DSHs may be due to the P25 film used. This could be related to the rutile content of the P25. We have tested a series of DSHs made with pure anatase  $\text{TiO}_2$  layers made from colloidal solution. These cells did not show improved fill factors; however, the colloid used was composed of particles with diameters around  $15\text{ nm}$ , significantly smaller than those in P25, which may also have caused a decrease in pore filling. We are attempting to fabricate pure anatase colloids with  $25\text{-nm}$  particles for comparison with those in P25.

In Table 1 we have also included data from a DSH constructed using electrodeposited ZnO, a phosphonated ruthenium dye, and electrodeposited CuSCN.<sup>23,24</sup> This

**Table 2. Measured Pore Filling by CuSCN Deposition from Propylsulfide for  $\text{TiO}_2$  Films of Different Thicknesses**

	sample no.			
	1	2	3	4
$\text{TiO}_2$ thickness ( $\mu\text{m}$ )	1.7	3	3.6	5.8
total CuSCN (mg)	1.6	2.0	0.84	1.8
CuSCN overlayer ( $\mu\text{m}$ )	2.1	2.6	0.16	1.25
CuSCN overlayer (mg)	1.1	1.3	0.08	0.66
CuSCN in pores (mg)	0.5	0.7	0.76	1.14
weight if filled (mg)	0.5	0.92	1.1	1.78
pore filling	100%	76%	70%	64%

type of cell shows a much higher  $\alpha$  (lower ideality factor) at full light than does that of the P25/dye/CuSCN cell. This results in a higher fill factor, even considering the large series resistance. About half of the series resistance of this cell was due to the low-conductivity  $\text{SnO}_2$  glass used (TEC 15). Corrected for this external resistance, the fill factor for the high light IV would be  $\approx 65\%$ . This shows that low fill factors are not intrinsic to the metal-oxide/dye/CuSCN interface.

**CuSCN Deposition.** The results shown above indicate that the solvent-based method of depositing CuSCN into mesoporous  $\text{TiO}_2$  is surprisingly successful given the low concentration of the solution. We find that a saturated CuSCN solution in propylsulfide is  $\approx 15\text{ mg/mL}$ , which gives a volume percentage of  $0.5\%$  (density  $\text{CuSCN} = 2.85\text{ g/cm}^3$ ). Table 2 gives the degree of pore filling achieved for four  $\text{TiO}_2$  films varying from  $1.7$  to  $5.8\text{ }\mu\text{m}$ . In the  $1.7\text{-}\mu\text{m}$  film we measure a pore filling near  $100\%$ ; however, it must be remarked that the error in the measurement is at least  $10\%$ . For the films between  $3$  and  $5.8\text{ }\mu\text{m}$ , the measured degree of pore filling is near  $70\%$ , apparently declining from  $76$  to  $64\%$  with increasing thickness.

The following idealized model helps describe the pore-filling process. Consider the application of one film containing  $1.2\text{ }\mu\text{L}$  of CuSCN solution to a  $5\text{-}\mu\text{m}$ -thick  $\text{TiO}_2$  film of  $1\text{ cm}^2$ , with  $60\%$  porosity. The  $1.2\text{ }\mu\text{L}$  of solution will contain  $18\text{ }\mu\text{g}$  of solid CuSCN. We observe that approximately two-thirds of the CuSCN is deposited on the active surface; the rest remains on the applying needle or is lost to edge effects. Thus,  $1.2\text{ }\mu\text{L}$  of solution will deposit  $12\text{ }\mu\text{g}$  of CuSCN. If this  $12\text{ }\mu\text{g}$  of CuSCN were to form a uniform layer on each  $\text{TiO}_2$  particle, the thickness of that layer would be only  $1\text{ \AA}$ . This is calculated using the specific surface area of the P25 powder ( $50\text{ m}^2/\text{g}$ ) and the thickness and porosity of the film. If each successive application of the solution adds a  $1\text{-\AA}$  coating to every particle, the process can continue until the necks between the pores become blocked. Additional CuSCN added then forms an overlayer above the porous  $\text{TiO}_2$  film.

To estimate how well the pores might be filled by such a process, consider a  $\text{TiO}_2$  film composed of  $25\text{-nm}$  particles on a cubic lattice. This film would have  $52\%$  porosity, slightly less porous than the P25 films used in this paper. A cubic lattice of  $25\text{-nm}$  particles gives rise to channels whose narrow points are  $10\text{ nm}$  across. As equal thickness layers are deposited on each particle, the growing films on each side will meet across the narrow point when the thickness of the coating on each particle is  $5\text{ nm}$ . Figure 6 illustrates this result with a diagonal cross section through the cubic lattice. When

(23) O'Regan, B.; Shklover, V.; Grätzel, M. *J. Electrochem. Soc.* **2001**, *148*, C498–C505.

(24) O'Regan, B.; Schwartz, D. T.; Zakeeruddin, S. M.; Grätzel, M. *Adv. Mater.* **2000**, *12*, 1263–1267.

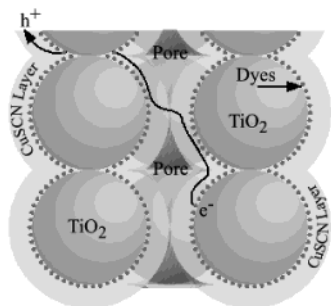


**Figure 6.** Cross section illustrating idealized pore filling by adding CuSCN layers to the surface of dye-sensitized TiO<sub>2</sub> particles on a cubic lattice.

the films meet and block the pore neck, they will leave a small unfilled space in the center of each cube of eight TiO<sub>2</sub> particles, in the shape of an indented bi-pyramid. The volume of this space is only 7% of the initial pore volume; thus, the maximum pore filling that can be achieved by adding successive uniform films to a cubic array of particles is 93%. (The cross section in Figure 6 appears to have a lower fraction of pore filling due to the fact that it intersects the unfilled space at its widest point.)

In fact, in thicker films we observe pore filling smaller than 93% for a number of reasons. Most importantly, it would be highly unlikely that our material makes a uniform deposition on each particle. Several trends oppose this. First would be the nucleation and growth of larger crystals which block entire pores before lower pores have filled. Cursory SEM investigation has not revealed evidence for larger crystals, but we are unable to resolve details of the material within the pores. Second, even without the growth of larger crystals, random spatial variation in the deposition from each solution application will tend to randomly block pore necks throughout the film. When all the pores surrounding a volume are blocked, further deposition in that volume will not occur. Since P25 is a polydisperse and highly aggregated material, the maximum theoretical pore filling will probably be smaller than 93%. It might also be expected that evaporation from the solvent surface would tend to favor precipitation on or near the surface of the TiO<sub>2</sub> film. However, our method of adding very small amounts of liquid seems to avoid this problem, as we do not see a steep decrease in pore filling with increasing film thickness. Further details of the solvent application procedure will be published elsewhere.

As a last caveat, it may be possible that most pore necks in the final TiO<sub>2</sub>/dye/CuSCN heterostructure are not fully closed. This would occur because as the TiO<sub>2</sub> film fills up with CuSCN, the evaporation rate of the propylsulfide from the surface, following the formation of one solvent layer, will start to compete with the flow of the solvent into the porous film through the remaining small pore necks. When the pore necks become very small, not enough solution will enter the porous film to deposit the CuSCN required to close the necks below the surface. In fact, just slightly open pores may be quite useful for the final drying of the film, as solvent trapped deep in the film will still be able to escape. In accordance with this model, we have seen a quite fast response of the photocurrent to the introduction of ammonia into the gas above the surface of the CuSCN.

**Effects of Drying.** As noted in a previous section, the final drying of the film appears to be critical. After the last layer of CuSCN solution is applied, the films are kept at 80 °C in air for a few minutes. Subsequently, they are treated for several hours at low vacuum ( $5 \times 10^{-2}$  mbar). During the vacuum treatment the films lose  $\approx 1\%$  of the total weight gained during the CuSCN deposition. We presume that this weight loss indicates the evaporation of additional propylsulfide, or water bound to the TiO<sub>2</sub>. Reflection IR spectra taken before vacuum drying do not show propylsulfide peaks; however, the sensitivity may simply be inadequate. Before and after drying, both XRD and IR show the peaks associated with the rhombohedral form of CuSCN, also known as  $\beta$ -CuSCN. The line widths of the XRD spectrum do not change markedly, indicating that the drying process is not accompanied by large-scale recrystallization of the CuSCN in the pores.

In comparing the characteristics of type A and type B cells, it was mentioned that the dissimilarities were due to differences in the CuSCN films. Since the two examples shown in Figures 2 and 3 were made, one after the other, with the same CuSCN solution, possible differences in the CuSCN layer are limited to the degree and homogeneity of the pore filling, the thickness of the overlayer, and the degree of drying. We have observed that variation in the overlayer (0.2–2  $\mu\text{m}$ ) does not cause obvious changes in the fill factor. We have also observed a tendency of some cells of type A to evolve to cells of type B with 1 to several weeks storage in dry argon. It is likely that these cells differ in the distribution of the CuSCN in the pores, and thus in the rate at which they can become completely dry. Differences in the CuSCN distribution may be caused by small changes in the way the first layers of CuSCN nucleate in the film. We have not yet optimized the CuSCN deposition parameters, outside of the temperature; thus, we expect that more complete and more homogeneous pore filling should be possible.

We have tested the homogeneity, across the surface, of two seemingly “intermediate” TiO<sub>2</sub>/N3/CuSCN cells by evaporating an array of 2-mm-diameter gold spots as back contacts. In each case the IV curves from the different gold spots were quite similar, with the photocurrent, fill factor, and voltage varying 10%, 3%, and 1%, respectively, from the mean. These data suggest, but do not prove, that the variation between A and B cells is due to specific, surface-wide, events related to the CuSCN deposition, rather than to variable deposition “success” across the surface. On the other hand, the 2-mm spot size may be too large relative to the existing surface inhomogeneity.

During the argon storage, an increase in fill factor is frequently correlated with a decrease in plateau photocurrent. One explanation for this trend is the following. The similarity of the IV evolution under vacuum and argon storage implies some last remaining propylsulfide or water is being removed under argon. As the solvent molecules are removed from the pores, the space they occupied must be filled with gas, as the mass and volume of the CuSCN is fixed. If the last propylsulfide or water is distributed as defects in the CuSCN crystals, the crystals themselves must shrink. This shrinkage could cause a small gap to open between the CuSCN

and the TiO<sub>2</sub>/dye surface along some parts of the pore periphery. This could leave some dyes completely disconnected from the CuSCN and therefore inactive for photocurrent generation. At the same time, the conductivity of the CuSCN network should improve and the recombination rate decrease for those areas where TiO<sub>2</sub>/dye/CuSCN contact still exists. These combined changes could give the improved fill factor, and yet decreased total photocurrent.

The changes in the IVs that accompany the drying are complex, and simply the physical removal of propylsulfide or water is probably not a sufficient explanation. It may turn out that Cu(I) atoms still ligated by propylsulfide provide hole traps and that the removal of the last propylsulfide results in a decrease in the trap density and an improvement in conductivity. It was noted above (Figure 3) that some cells with higher fill factors show photocurrents which are nonlinear with respect to light level and that the nonlinearity cannot be ascribed to the series resistance. Another possible source of nonlinearity is direct quenching of the excited state of the dye by the holes in CuSCN. A hole trapped in CuSCN will bear some similarity to a Cu(II) ion in solution. We have observed that Cu(II) ions are effective quenchers of N3 luminescence in homogeneous solution. The concentration and distribution of trapped holes will depend critically on the conditions at the TiO<sub>2</sub>/dye/CuSCN interface, which will presumably be quite sensitive to the removal of the last few volatile molecules. Further research is underway concerning the drying step.

We have not begun to seriously investigate the stability of these TiO<sub>2</sub>/dye/CuSCN cells under illumination, either sealed or exposed to air. Initial tests with light exposure, open to air, show some promise. After 9 h of illumination with 1000 W/m<sup>2</sup>, simulated AM1.5, the photocurrent of some cells decreased only 1.5%, whereas others went up more than 10%. On the other hand, other cells exposed to  $\approx 1000$  W/m<sup>2</sup> illumination with almost no UV content showed a decrease in photocurrent of 35%. At this point, the stability seems to be determined by the drying history of the cell, with longer argon drying resulting in more stable cells. In addition, cells with an evaporated gold layer seem more stable.

This could be due to the sealing effect of a gold layer or to the mild heating in high vacuum that occurs during the gold evaporation.

### Future Prospects

The results shown above indicate that CuSCN remains a promising hole conductor for solid-state dye-sensitized cells. Many parts of the fabrication have not yet been optimized and therefore we expect that the efficiency can be improved significantly. We have not yet optimized parameters in the CuSCN deposition such as the solution concentration, speed of spreading, or gas flow across the surface. Improvements in the CuSCN deposition should allow a reduction of the difference between the equivalent liquid-junction cell and the CuSCN cell. Improvements in the voltage can be expected from the control of the surface charge via materials such as *tert*-butylpyridine<sup>16</sup> and tunnel barriers.<sup>25</sup> Photocurrent should increase with the use of thicker TiO<sub>2</sub> films and light management techniques, as already applied in the dye-sensitized liquid-junction cells. The N3 dye used for the results reported herein has been optimized for use in iodine/iodide electrolyte and thus is not necessarily the best absorber for solid-state sensitized cells. Initial results show that merocyanines, porphyrins, and rhodamines can give significant photocurrents in the TiO<sub>2</sub>/dye/CuSCN interface. Last, it should be possible to use inorganic absorbers with very high absorption coefficients, such as PbS, which have been shown to sensitize TiO<sub>2</sub> but which are not stable in the electrolyte cells.<sup>26</sup> On the other hand, it remains to be seen if the fill factors in these cells can be brought up to acceptable levels. This may require the change to another oxide, such as ZnO, and/or a better understanding of the mechanisms of recombination and charge transport in the interpenetrating metal-oxide/CuSCN structure.

CM020572D

(25) Tennakone, K.; Bandara, J.; Bandaranayake, P. K. M.; Kumara, G. R. A.; Konno, A. *Jpn. J. Appl. Phys., Part 2* **2001**, *40*, L732–L734.

(26) Vogel, R.; Hoyer, P.; Weller, H. *J. Phys. Chem.* **1994**, *98*, 3183–3188.